ChemComm

COMMUNICATION

View Article Online
View Journal | View Issue

Cite this: *Chem. Commun.*, 2015, 51, 499

Received 16th September 2014,
Accepted 7th November 2014

DOI: 10.1039/c4cc07306a

www.rsc.org/chemcomm

Published on 10 november 2014. Downloaded on 2025. 08. 26. 14:59:25.

A seed-engineering approach toward a hollow nanoreactor suitable for the confined synthesis of less-noble Ni-based nanocrystals†

Kwanyong Jeong, Soo Min Kim and In Su Lee*

A hollow nanoreactor suitable for the cultivation of Ni-nanocrystals was developed through a distinct seed-engineering stratagem, which involved the assembly of a catalytically active Au/Pd-heterojunction-nanocrystal inside the hollow silica nanoshell. The resulting hollow nanoreactor demonstrated a targeted performance in the cavity-confined growth of the catalytic Ni nanocrystal.

Yolk@shell nanoparticles, which carry a functional core inside a hollow and porous nanoshell, are attractive candidates for nanoreactors that allow spatially confined reactions for selectively internalized molecules.[1] Most research efforts to date have focused on developing highly durable and recyclable nanocatalyst systems that efficiently and selectively catalyze the transformation of organic molecules.[2,3] Very recently, a new angle of approach has been suggested by a few researchers to utilize hollow nanoreactors for synthesizing and decorating nanoparticles within the confines of the protected interior space.[4] For instance, we recently devised the nanoreactor approach for templating the synthesis of noble metal nanocrystals, such as Pt, Ag, Au and their alloys, through exploitation of the seed-mediated growth inside the cavity of Au-seed containing hollow silica nanospheres, **Au@*h*-SiO$_2$**.[5] The hollow nanoreactor-based approach has enabled the production of ligand-free noble-metal nanocrystals with well-controlled morphologies from a highly concentrated suspension. In this context, the current study was performed with the aim of further extending the utility of the hollow nanoreactors toward the production of less confinable non-noble metal nanocrystals beyond the noble metals. Unlike noble metals that can be easily restricted to grow on Au-seeds using mild reducing agents, the growth of less reducible non-noble metals is more complicated as it requires severe reaction conditions, which results in its homogenous nucleation in the bulk solution. In particular, this study focuses on devising a hollow nanoreactor suitable for the cultivation of Ni-nanocrystals, which plays important roles as versatile and representative non-noble metal catalysts in many applications.[6] Herein, we report our strategy for engineering a seeding core toward the Ni-growing nanoreactor, which includes an assembly of a catalytically active Au/Pd-heterojunction-nanocrystal inside the hollow silica nanoshell. The nanoreactor-synthesized Ni-nanocrystals exhibited an active and recyclable performance in catalyzing hydrogen generation from NH_3BH_3 and the chemoselective reduction of nitroarenes in aqueous solutions at room temperature. Moreover, we demonstrate the usefulness of these hollow nanoreactors in the synthesis and post-modification of Ni-based hybrid nanocrystals.

Firstly, the employability of the previously developed **Au@*h*-SiO$_2$** was investigated in growing Ni nanocrystals. $NiCl_2$ in a suspension of **Au@*h*-SiO$_2$** was treated with a range of mild reducing agents, including ascorbic acid, H_2O_2, and hydrazine. Although these reducing agents had previously allowed the Au-seed-mediated growth of Au,[5a] Pt,[5b] and Ag,[5c] respectively, it did not lead to the reduction of Ni^{2+}. An alternative trial with a stronger reducing agent, $NaBH_4$, caused Ni deposition on the Au seed. However, this process also formed undesirably large Ni particles on the outer surface of the **Au@*h*-SiO$_2$** nanoreactor (Fig. S1, ESI†). This preliminary study suggested that a more powerful seed needs to be engineered for restricting the Ni growth to the interior of the hollow nanoreactor. Therefore, a strategy was planned to introduce Pt, Pd, or Ni, which is known to catalyze the reductive decomposition of Ni^{2+}–hydrazine complex,[7] as a seeding material by incorporating Pt^{2+}, Pd^{2+}, or Ni^{2+} ions into the reductive dissolution process of the Fe_3O_4, which had been adopted previously for hollowing the **(Fe_3O_4/Au)@SiO$_2$** into **Au@*h*-SiO$_2$**.[5c] It was hypothesized that *in situ* reduced Pt, Ni, or Pd would be deposited on the Au-nanocrystal inside the cavity during the hollowing process (Scheme 1).

The incorporation of Ni^{2+}, Pt^{2+}, and Pd^{2+} ions was carried out by adding aliquots of $Ni(NO_3)_2$, Na_2PtCl_4, and Na_2PdCl_4 solutions, respectively, into the microemulsion suspension which had previously been used to prepare **(Fe_3O_4/Au)@SiO$_2$** (for the detailed procedure, refer to the experimental section in ESI†). The transmission electron microscopy (TEM) images showed that all reactions afforded similar core@shell structures, which contain an embedded

Department of Chemistry, Pohang University of Science and Technology (POSTECH), Gyeongbuk, 790-784, Korea. E-mail: insulee97@postech.ac.kr

† Electronic supplementary information (ESI) available: More experimental data including TEM images. See DOI: 10.1039/c4cc07306a

Published on 10 November 2014. Downloaded on 2025. 08. 26. 14:59:25.

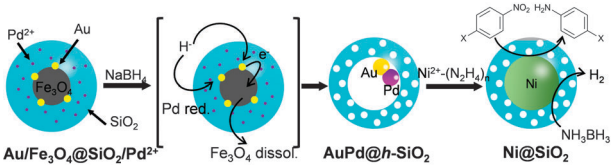

Scheme 1 The synthetic strategy of the Ni-growing **(Au/Pd)@*h*-SiO$_2$** nanoreactor.

hybrid nanocrystal, composed of a Fe_3O_4 nanocrystal and surrounding satellite nanocrystals, at the core of the silica nanosphere (Fig. 1a–c). The control reactions without tetraethyl orthosilicate (TEOS) revealed that a comparable amount of Pt and Au were present around the Fe_3O_4 nanoparticle in isolated nanoparticles. Conversely, only a small amount of Ni and Pd were detected around the Fe_3O_4 nanoparticle (Fig. S2, ESI†). Additional control experiments, excluding both $HAuCl_4$ and TEOS, showed a sparse population of Pt element on the isolated nanoparticles (Fig. S3, ESI†). From these observations, it can be deduced that, in the resultant core@shell nanospheres, the Ni^{2+} and Pd^{2+} ions were dispersed throughout the silica shell, generating **(Fe_3O_4/Au)@(SiO_2/Ni^{2+})** and **(Fe_3O_4/Au)@(SiO_2/Pd^{2+})** nanospheres, respectively. In contrast, the Pt^{2+} ions were co-included as the components of satellite nanocrystals together with Au surrounding the Fe_3O_4 nanocrystal, resulting in the formation of a **(Fe_3O_4/AuPt^{2+})@SiO_2** nanosphere. When the resultant nanospheres were exposed to a solution of $NaBH_4$, which is expected to reductively dissolve the Fe_3O_4 and simultaneously reduce the metal ions, they were found to undergo different reactions depending on the incorporated ions, Pt^{2+}, Ni^{2+}, and Pd^{2+}. In the case of **(Fe_3O_4/AuPt^{2+})@SiO_2**, it was found that the Fe_3O_4 core was not subject to the expected reductive dissolution. This was presumably due to the reduced catalytic activity of the attached Au nanocrystal, which alloyed with Pt. The $NaBH_4$ treatment therefore afforded an unexpected nanostructure, **(Fe_3O_4/AuPt)@*h*-SiO_2**, in which a satellite-type nanoparticle, consisting of a 9(±1) nm-sized Fe_3O_4 core and surrounding Au/Pt bimetallic nanocrystals of 2.1(±0.5) nm size, is placed inside the 19(±2) nm-sized internal cavity, which was developed through silica etching (Fig. 1e). The interior cavity of the **(Fe_3O_4/AuPt)@*h*-SiO_2**, which was partially occupied by the undissolved Fe_3O_4 core, was regarded as unsuitable for metal growth. In comparison, when **(Fe_3O_4/Au)@(SiO_2/Ni^{2+})** was immersed in a $NaBH_4$ solution, the Fe_3O_4 core dissolved rapidly due to the reductive dissolution process, facilitated by the attached Au-nanocrystals, while the Ni^{2+} ions slip away from the silica through *in situ* generated small pores. Therefore, regardless of the content of the initially incorporated Ni^{2+} ions in the silica shell, the reaction yielded a nanorattle-like structure containing a spherical Au core, **Au@*h*-SiO_2**, which was found to be almost identical to the one previously prepared from **(Fe_3O_4/Au)@SiO_2** (Fig. 1d and Fig. S4, ESI†). When **Fe_3O_4@SiO_2/M^{2+}** (M = Ni, Pd, Pt) nanospheres, which were prepared without containing Au nanocrystals, were treated with $NaBH_4$ solution for the purpose of control, the removal of the Fe_3O_4 core was not observed from any nanosphere, which indicates little effect of metal ions other than the Au nanoparticle on the reductive dissolution process (Fig. S5, ESI†).

The $NaBH_4$ treatment of the **(Fe_3O_4/Au)@(SiO_2/Pd^{2+})** also generated a similar nanorattle-like structure. This consisted of a 21(±2) nm-sized cavity and an encaged tiny core nanocrystal which appeared ellipsoidal in TEM images rather than spherical (Fig. 1f). Further investigation using high resolution-TEM (HR-TEM), STEM, and energy-dispersive X-ray spectroscopy (EDX) identified the ellipsoidal core to be an Au/Pd-heterodimer-nanocrystal with a dumbbell-like structure that includes spherical Au and Pd grains of a similar size (*ca.* 2.5 nm) joined by a small interfacial area (Fig. 2d). The above-identified structure of the **(Au/Pd)@*h*-SiO_2** represents the successful introduction of the reduced Pd into the cavity of the hollow silica nanoshell, as outlined in the initial synthetic strategy. Time-course TEM and HR-TEM studies revealed that the Fe_3O_4 at the core of the **(Fe_3O_4/Au)@(SiO_2/Pd^{2+})** was dissolved very early in the reaction (within 10 min), leaving a spherical Au-nanocrystal in the newly formed interior cavity (Fig. 2a). Whilst the cavity expanded gradually over the reaction period, from 12(±1) nm at 10 min to 21(±2) nm at 1 h, the Pd, as seen in the STEM images, continuously and gradually migrated

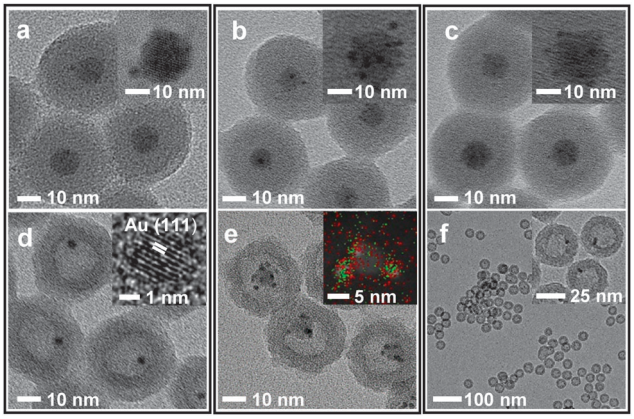

Fig. 1 TEM and HRTEM (insets) images of (a) **(Fe_3O_4/Au)@(SiO_2/Ni^{2+})**, (b) **(Fe_3O_4/AuPt^{2+})@SiO_2** and (c) **(Fe_3O_4/Au)@(SiO_2/Pd^{2+})** core@shell nanospheres and (d) **Au@*h*-SiO_2** (e) **(Fe_3O_4/AuPt)@*h*-SiO_2** (insets: EDX elementary maps, Au (red), Pt (green)) and (f) **(Au/Pd)@*h*-SiO_2** yolk@shell nanospheres, which were produced by treating the core@shell nanospehres with $NaBH_4$.

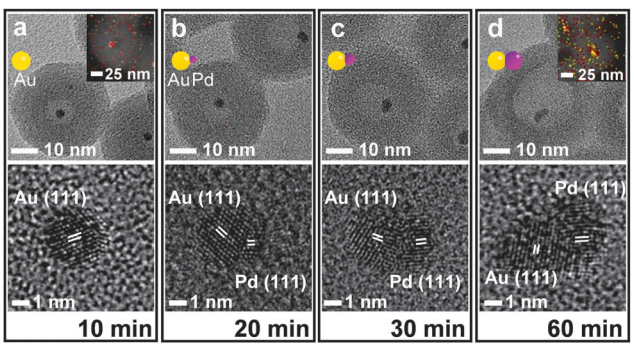

Fig. 2 TEM (upper) and HRTEM (lower) images of samples isolated during the reaction of the **(Fe_3O_4/Au)@(SiO_2/Pd^{2+})** with $NaBH_4$ at (a) 10, (b) 20, (c) 30, and (d) 60 min, respectively. Insets: EDX elementary maps for showing the distribution of Au (red) and Pd (yellow) elements.

This journal is © The Royal Society of Chemistry 2015

Published on 10 november 2014. Downloaded on 2025. 08. 26. 14:59:25.

inward toward the Au-seed. This nucleated a Pd grain on the Au seed at 20 min; the grain eventually proliferated to a size of 4.9(±0.8) nm (Fig. 2 and Fig. S6, ESI†). It can be deduced that the reduced Pd was gradually released inward from the hollowed silica, which was continuously bored from within, and deposited on the pre-existing Au nanocrystal in the internal cavity. When the preparation of **(Au/Pd)@*h*-SiO$_2$** was attempted using an increased content of silica-incorporated Pd^{2+} ions, the Pd grain of the resulting Au/Pd-core-nanocrystal was found to increase in size, while maintaining the size of the Au grain (Fig. S7, ESI†).

The nanorattle-like structure of the **(Au/Pd)@*h*-SiO$_2$**, bearing a catalytically active Pd grain as part of the internal core, signifies the formation of the targeted nanoreactor framework which guides the reduction of the Ni^{2+}–hydrazine complex to occur inside the cavity, thus spatially confining the synthesis of Ni nanocrystals. A pre-mixed aliquot of $NiCl_2$ and hydrazine was added to an aqueous suspension containing the **(Au/Pd)@*h*-SiO$_2$** in a capped vessel with constant stirring at 45 °C.[7a] The color of the suspension slowly changed from violet to light brown during the initial 20 min of the reaction, and then instantly changed to black with effervescence. The TEM and STEM images of the isolated black powder after a reaction time of 1.5 h revealed the confined growth of a 23(±3) nm Ni nanocrystal exclusively on the inside of the hollow cavity, creating a **Ni@SiO$_2$** core@shell structure in which a reduced Ni grown on the Au/Pd core was compacted within the porous silica nanoshell (Fig. 3a). HRTEM and XRD analyses confirmed the formation of a polycrystalline Ni nanoparticle with a face-centered-cubic (fcc) crystalline phase (Fig. 3b and c). Field dependent magnetization measurements show **Ni@SiO$_2$** exhibited superparamagnetic and ferromagnetic behaviors at 300 K and 5 K, respectively (Fig. S8, ESI†). The time-course TEM images showed that 24% of the hollow nanoreactors were filled by the Ni growth at 20 min, and as the reaction proceeded, the number of **(Au/Pd)@*h*-SiO$_2$** that transformed into **Ni@SiO$_2$** increased, reaching a conversion yield of 94% at 1.5 h (Fig. S9, ESI†). These observations suggest that the nucleation of the Ni was initiated on the surface of the Pd grain, which catalyzed the decomposition of the Ni^{2+}–hydrazine complexes, and the subsequent crystal growth was significantly boosted on the Ni nuclei.

To prove the effectiveness of the synthesized **Ni@SiO$_2$** in catalysis, we examined its catalytic performance in the hydrolytic dehydrogenation of NH_3BH_3 (ammonia borane, AB), which is required in high-performance hydrogen storage and generation

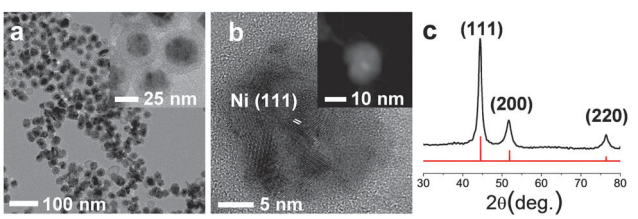

Fig. 3 (a) TEM, (b) HRTEM and STEM-HAADF (inset) images and (c) XRD pattern of the **Ni@SiO$_2$**. The red line in (c) shows the position of the reflections corresponding to the fcc Ni phase (JCPDS Card No. 01-1260).

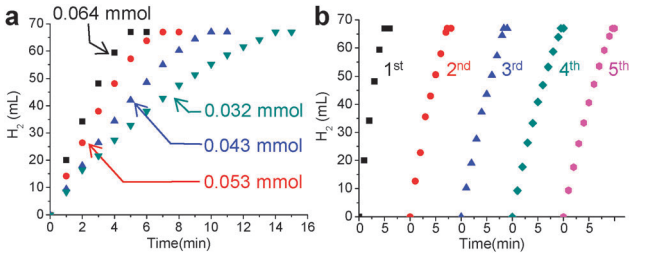

Fig. 4 Plots of volume of hydrogen generated *vs.* time for catalytic hydrolysis of AB (a) at various concentrations of the **Ni@SiO$_2$** catalyst and (b) during the recycling experiment.

systems.[8] Fig. 4a displays time-course curves of the hydrogen released of AB (2 M, 2 mL) during hydrolysis at room temperature by the **Ni@SiO$_2$** catalyst. The experiment was conducted with various Ni/AB molar ratios from 0.064 to 0.032, which generated stoichiometric amounts of hydrogen (67 mL, 3 mmol) in less than 15 min. The reaction rate of each curve was almost linearly dependent on the Ni/AB molar ratio, resulting in consistent turnover frequency (TOF) values among the curves. The average TOF of the **Ni@SiO$_2$** catalyst (8.0 min^{-1}), calculated on the basis of the total moles of Ni, is somewhat lower than the reported highest value (30.7 min^{-1}) for 6.5 nm-sized surfactant-free Ni nanoparticles.[8b] However, when defined as the moles of hydrogen generated per unit surface area of Ni nanocrystals, the TOF of the **Ni@SiO$_2$** catalyst (4.6×10^{-18} mol min^{-1} nm^{-2}) is considered to be comparable to the highest reported value (5.02×10^{-18} mol min^{-1} nm^{-2}), which implies high catalytic activity and well-exposedness of the surfactant-free surface of the Ni nanocrystal grown inside the porous silica nanoshell. Reuse of the magnetically recovered **Ni@SiO$_2$** did not result in a significant decline in the catalytic activity over five consecutive runs (Fig. 4b). The usefulness of the **Ni@SiO$_2$** catalyst was investigated further in the industrially important catalytic reduction of nitroarenes, which was recently carried out by using a Ni nanocatalyst in an aqueous solution at room temperature and using environment-friendly hydrazine as a reducing agent (Table S1, ESI†).[9] A trial reaction of *p*-nitroaniline (0.1 M) and hydrazine (4 M) with 15 mol% of **Ni@SiO$_2$** was carried out in water at room temperature. The product, *p*-diaminobenzene, was afforded in a quantitative yield within 30 min, and this showed a higher TOF (13 h^{-1}) than that of the reported *ca.* 10 nm-sized Ni nanoparticles (10 h^{-1}). The **Ni@SiO$_2$** catalysts were well dispersed in the stirred reaction suspension, and after the reaction was completed, they could be readily retrieved using a small magnet (Fig. S10, ESI†). The reusability tests showed that the magnetically recovered catalyst retained most of its initial activity in terms of conversion yield and selectivity over three consecutive reactions. The same reaction performed using various functionalized nitroarenes also led to the complete conversion of substrates in less than 4 h. More importantly, while catalyzing the transformation of the nitro groups to the amino groups with a high TOF, the **Ni@SiO$_2$** did not much affect other functional groups (halogen, ether, carbonyl-, or alkenyl-groups) and predominantly afforded the corresponding substituted anilines with

Published on 10 november 2014. Downloaded on 2025. 08. 26. 14:59:25.

a selectivity higher than 83%. The remarkable chemoselectivity of the **Ni@SiO$_2$** toward the reduction of nitro groups may be attributed to the mild reaction conditions, at room temperature and using a using weak reducing agent, which is allowed by the surfactant-free catalytic surface of the Ni nanocrystals protected by the porous silica shell.

In addition to the synthesis of the Ni nanocrystals, the hollow nanoreactor engineered in this study was also applicable to the fabrication of alloy nanocrystals.[10] Therefore, an additional injection of a mixture of $CoCl_2$ and hydrazine into the Ni-growing suspension containing the **(Au/Pd)@*h*-SiO$_2$** and Ni^{2+}–hydrazine complex led to the co-reduction of Co^{2+} together with Ni^{2+}. This led to the consequent growth of a Ni/Co alloy nanocrystal inside the cavity, producing a **(Ni/Co)@SiO$_2$** nanosphere with a core@shell-type structure (Fig. S11, ESI†). The control reaction with Co^{2+}– or Fe^{2+}–hydrazine complexes and the **(Au/Pd)@*h*-SiO$_2$** suspension did not generate any reduced Co or Fe species, implying that the pre-grown Ni surface is responsible for reducing the Co^{2+} complex and forming the Ni/Co alloy. Meanwhile, the successive addition of $CuCl_2$ solution and hydrazine to the **(Au/Pd)@*h*-SiO$_2$** suspension led to the homogeneous nucleation and the generation of large Cu particles at the outside solution of the hollow nonreactor. The annealing process of the synthesized **(Ni/Co)@SiO$_2$** at temperatures as high as 700 °C led to an alteration in the morphology and crystallinity of the Ni/Co nanocrystal coated by the thermally stable silica shells, hence preserving their nanocrystalline nature (Fig. S11, ESI†). This allowed the post-synthetic modification of the hollow nanoreactor-synthesized nanocrystals.

In summary, a hollow nanoreactor suitable for templating the synthesis of less reducible and, therefore, less-confinable Ni nanocrystals was developed through a seed-engineering strategy which involved introducing a catalytically active material on the seed entrapped within a hollow silica nanoshell. The Au/Pd-heterojunction-nanocrystal-bearing nanoreactor demonstrated targeted reduction of Ni^{2+}–hydrazine complexes and consequent growth of the Ni nanocrystals within the confines of its cavity. The usefulness of the nanoreactor-synthesized Ni nanocrystals was verified by catalyzing the hydrogen generation of NH_3BH_3 and chemoselective reduction of nitroarenes in the aqueous phase and at room temperature. Moreover, we demonstrated the extendable utility of the hollow nanoreactors in the synthesis and post-modification of alloy nanocrystals.

This work was supported by the National Research Foundation of Korea (NRF) grant funded by the Korea government (MEST) (2011-0017377).

Notes and references

1 For general reviews on yolk@shell-type nanoparticles, (*a*) J. Liu, S. Z. Qiao, J. S. Chen, X. W. Lou, X. Xing and G. Q. Lu, *Chem. Commun.*, 2011, **47**, 12578–12591; (*b*) X.-J. Wu and D. Xu, *Adv. Mater.*, 2010, **22**, 1516–1520; (*c*) Y. Zhao and L. Jiang, *Adv. Mater.*, 2009, **21**, 3621–3638.

2 For reviews on hollow nanoreactor-based catalytic systems, (*a*) Y. Li and J. Shi, *Adv. Mater.*, 2014, **28**, 3176–3205; (*b*) X. Li, Y. Yang and Q. Yang, *J. Mater. Chem. A*, 2013, **1**, 1525–1535; (*c*) M. Pérez-Lorenzo, B. Vaz, V. Salgueiriño and M. A. Correa-Duarte, *Chem. – Eur. J.*, 2013, **19**, 12196–12211; (*d*) Q. Zhang, I. Lee, J. B. Joo, F. Zaera and Y. Yin, *Acc. Chem. Res.*, 2013, **46**, 1816–1824.

3 Recent examples of hollow nanoreactor-based catalytic systems, (*a*) G.-H. Wang, J. Hilgert, F. H. Richter, F. Wang, H.-J. Bongard, B. Spliethoff, C. Weidenthaler and F. Schüth, *Nat. Mater.*, 2014, **13**, 293–300; (*b*) S. M. Kim, M. Jeon, K. W. Kim, J. Park and I. S. Lee, *J. Am. Chem. Soc.*, 2013, **135**, 15714–15717; (*c*) X. Fang, Z. Liu, M.-F. Hsieh, M. Chen, P. Liu, C. Chen and N. Zheng, *ACS Nano*, 2012, **6**, 4434–4444; (*d*) Y. Yang, X. Liu, X. Li, J. Zhao, S. Bai, J. Liu and Q. Yang, *Angew. Chem., Int. Ed.*, 2012, **51**, 9164–9168.

4 (*a*) M. Xiao, C. Zhao, H. Chen, B. Yang and J. Wang, *Adv. Funct. Mater.*, 2012, **22**, 4526–4532; (*b*) M. Sanlés-Sobrido, M. Pérez-Lorenzo, B. Rodríguez-González, V. Salgueiriño and M. A. Correa-Duarte, *Angew. Chem., Int. Ed.*, 2012, **51**, 3877–3882; (*c*) J. Lian, Y. Xu, M. Lin and Y. Chan, *J. Am. Chem. Soc.*, 2012, **134**, 8754–8757; (*d*) S. Ding, J. S. Chen, G. Qi, X. Duan, Z. Wang, E. P. Giannelis, L. A. Archer and X. W. Lou, *J. Am. Chem. Soc.*, 2011, **133**, 21–23; (*e*) L. Tan, D. Chen, H. Liu and F. Tang, *Adv. Mater.*, 2010, **22**, 4885–4889.

5 (*a*) T.-L. Ha, J. Shin, C. W. Lim and I. S. Lee, *Chem. – Asian J.*, 2012, **7**, 36–39; (*b*) K. M. Yeo, S. H. Choi, J. W. Kim and I. S. Lee, *Angew. Chem., Int. Ed.*, 2011, **50**, 745–748; (*c*) K. M. Yeo, J. Shin and I. S. Lee, *Chem. Commun.*, 2010, **46**, 64–66.

6 (*a*) C.-J. Liu, J. Ye, J. Jiang and Y. Pan, *ChemCatChem*, 2011, **3**, 529–541; (*b*) H.-L. Jiang and Q. Xu, *Catal. Today*, 2011, **170**, 56–63; (*c*) F. Alonso, P. Riente and M. Yus, *Acc. Chem. Res.*, 2011, **44**, 379–391.

7 (*a*) M. Grzelczak, J. Pérez-Juste, B. Rodríguez-González, M. Spasova, I. Barsukov, M. Farle and L. M. Liz-Marzán, *Chem. Mater.*, 2008, **20**, 5399–5405; (*b*) M. Grzelczak, B. Rodríguez-González, J. Pérez-Juste and L. M. Liz-Marzán, *Adv. Mater.*, 2007, **19**, 2262–2266; (*c*) S.-H. Wu and D.-H. Chen, *J. Colloid Interface Sci.*, 2003, **259**, 282–286; (*d*) M. S. Hegde, D. Larcher, L. Dupont, B. Beaudoin, K. Tekaia-Elhsissen and J. M. Tarascon, *Solid State Ionics*, 1997, **93**, 33–50.

8 (*a*) M. Yadav and Q. Xu, *Energy Environ. Sci.*, 2012, **5**, 9698–9725; (*b*) P.-Z. Li, A. Aijaz and Q. Xu, *Angew. Chem., Int. Ed.*, 2012, **51**, 6753–6756; (*c*) Ö. Metin, V. Mazumder, S. Özkar and S. Sun, *J. Am. Chem. Soc.*, 2010, **132**, 1468–1469.

9 (*a*) R. K. Rai, A. Mahata, S. Mukhopadhyay, S. Gupta, P.-Z. Li, K. T. Nguyen, Y. Zhao, B. Pathak and S. K. Singh, *Inorg. Chem.*, 2014, **53**, 2904–2909; (*b*) H.-U. Blaser, H. Steiner and M. Studer, *ChemCatChem*, 2009, **1**, 210–221.

10 (*a*) A. K. Singh and Q. Xu, *ChemCatChem*, 2013, **5**, 652–676; (*b*) D. Wang and Y. Li, *Adv. Mater.*, 2011, **23**, 1044–1060.

 This journal is © The Royal Society of Chemistry 2015